31st Annual International Conference of the IEEE EMBS
Minneapolis, Minnesota, USA, September 2-6, 2009

Spatial Sensitivity of Near-Infrared Spectroscopic Brain Imaging Based on Three-Dimensional Monte Carlo Modeling

Chemseddine Mansouri, and Nasser H. Kashou

Abstract—**Accurate estimation of the radiation distribution in the adult human head requires realistic head models generated from magnetic resonance imaging (MRI) scans with true optical properties of each layer of the head. In this study, a complex three-dimensional structural data obtained by MRI are introduced in a three-dimensional Monte Carlo code, with varying optical properties and arbitrary boundary condition, to calculate the spatial sensitivity profile of photon in head, so-called banana-shaped. It is therefore a better model to incorporate the contribution of cerebrospinal fluid (CSF) when modeling the head. The spatial sensitivity of near-infrared spectroscopy measurement to regions in the brain, as well as the effect of optical fiber arrangement on the regions of measurement are investigated. It is shown that the detected signal in brain imaging measurements is greatly affected by the heterogeneity of the head tissue and its scattering properties.**

I. INTRODUCTION

Near-infrared spectroscopy (NIRS) allows the non-invasive investigation of the human brain and can complement other modalities such as functional magnetic resonance imaging (MRI) or positron emission tomography (PET) [1]. Several theoretical and experimental studies have been performed to investigate the propagation of light in various head models based on inhomogeneous structure. These models consist of multiple layers, such as the scalp, the skull, cerebrospinal fluid (CSF) and the brain, which can be divided into the gray and white matters. Okada *et al*. [2] employed models consisting of three and four-layered slabs and analyzed the photon propagation by both Finite Element method (FEM) based on diffusion theory and Monte Carlo (MC) calculations. Barnett *et al*. [3] and Custo *et al*. [4] used a three-dimensional head model, provided by MRI, employing a three-dimensional Finite-Difference code (FD) based on the diffusion theory and a three-dimensional MC code based on the transport equation, respectively, to study the effects of CSF scattering values on near-infrared light propagation in the adult head. Recently Heiskala *et al.* [5] used a three-dimensional head model combining anatomical and diffusion tensor MRI to investigate the effects of tissue anisotropy in the infant head.

The determination of optical properties (absorption coefficient μ_a and reduced scattering coefficient μ_s') of the brain in Near-Infrared Spectroscopy (NIRS) is important in many fields of medicine and neuroscience, both for monitoring physiologically important processes and for localizing brain activities. Since absorption of the activated region varies by changes in the blood volume and oxygenenation, one can measure brain activation by detecting the intensity change of near-infrared light passes through the brain [6]-[8]. However, estimating of the spatial sensitivity of the detected signal to a specific regions of the brain can be complicated because of the complex layered structure of the head and in particular the presence of the cerebrospinal fluid (CSF) filling the space between the skull and the brain. Although a number of theoretical and experimental investigations on NIR light propagation in the human head have been performed, knowledge of which region in the brain is sampled by NIR light remains incomplete. In our previous study [9] we simulated the time-resolved reflectance profiles and estimated absorption coefficient of the brain, on a semi-infinite three-layer structure, using only two-dimensional finite element and Monte Carlo codes. In this paper, for a better interpretation of data, we calculated the well known banana-shaped photon distribution on realistic three-dimensional based MRI head models. We used a three-dimensional Monte Carlo code in order to study the spatial sensitivity of the NIRS brain measurement to deep tissues.

II. METHODS

A. Head Model

We used segmented MRI data of an adult human head that we employed for 3D MC simulations. Fig. 1 shows the axial slice of the anatomical MRI, segmented into five tissue types (air, scalp, CSF, and gray/white matter). The whole volume was contained within 128 mm x 128 mm x 97 mm voxels with 1 mm3 of resolution. The limitation of the existing automatic methods used for image segmentation lies in the fact that they do not allow a correct differentiation of various types of the head structure because of the problem of contrast. To overcome this problem, we started initially with

Manuscript received April 23, 2009. This work was part of collaboration between Laboratoire LPMI-EA 1427, Arts et Métiers-ParisTech, Angers-France and The Children's Radiological Institute, Nationwide Children's Hospital, Columbus, OH 43205, USA.

C. Mansouri is with Laboratoire LPMI-EA 1427, Art et Métiers-Paris Tech 49035 Angers, France (phone: +33-(0)2-41-96-65-34; fax: +33-(0)2-41-96-65-11; e-mail: cmansouri@isaip.uco.fr).

N. H. Kashou is with The Children's Radiological Institute, Nationwide Children's Hospital, 700 Children's Drive, Columbus, OH 43205 USA (e-mail: nhkashou@ieee.org).

a preliminary automatic segmentation by using the available software BrainSuite2.0 (BrainSuite.usc.edu), and then we carried out a manual segmentation (by hand) under MATLAB for final identification of tissue compartments. This procedure was time consuming but it allows a greater level of detail to be applied to thin structures, such as the skull and cerebrospinal fluid (CSF). Thereafter, the values of the optical properties, presented in Table I, will be associated with each tissue type constituting the anatomical model. The light source adjacent to two detectors were placed on the transaxial plane, as illustrated in Fig.1, at different interfiber distances S-D1 and S-D2 of 20 mm and 34 mm respectively.

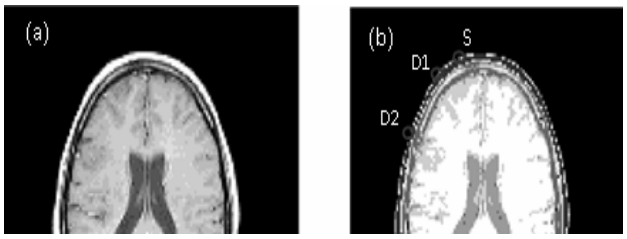

Fig. 1. (a) Anatomical MRI 3D head model. (b) Segmentation of the Anatomical MR image (a).

TABLE I
OPTICAL PROPERTIES OF THE MRI SEGMENTED HEAD MODEL

Tissue Type	μ_a [mm^{-1}]	μ_s' [mm^{-1}]	g	n
Scalp	0.018	1.0	0.9	1.3
Skull	0.021	0. 91	0.9	1.3
CSF	0.002	0.01,1.0	0.9	1 .3
Gray matter	0.0183	0.74	0.9	1.3
White matter	0.0165	0.98	0.9	1.3

B. Monte Carlo Method

We performed 3D MC simulations based on the head model displayed in Fig. 1. We used the Monte Carlo code developed by Wang and Jacques [10], which we have modified to calculate banana-shaped photon distribution in three-dimensional space.

The standard MC code proceeds in the following way: First, a photon packet is launched into the medium at the defined source position with an initial survival weight w that indicates the probability of a photon's successively propagation without absorption.

After each scattering event, a new direction of photon is calculated using the Henyey-Greenstein scattering function P (the probability distribution for the cosine of the deflection angle cosθ) defined as [10]:

$$p(\cos\theta) = \frac{1}{4\pi}\frac{1-g^2}{(1+g^2-2g\cos\theta)^{3/2}} \quad (1)$$

here θ is the deflection angle $\theta \in [0,\pi]$; the scattering anisotropy factor g equals $\langle \cos\theta \rangle$ and has a value between –1 and 1. A value of 0 indicates isotropic scattering and a value near 1 indicates very forward directed scattering.

A new scattering length is then determined from an exponential distribution $exp(-\mu_a L_m)$ where L is the length travelled by the photon in region m. Snell's law and Fresnel reflection formulas were applied at each boundary, when the photon does try to leave the medium [10]:

$$R(\theta_i) = \frac{1}{2}\left[\frac{\sin^2(\theta_i-\theta_t)}{\sin^2(\theta_i+\theta_t)} + \frac{\tan^2(\theta_i-\theta_t)}{\tan^2(\theta_i+\theta_t)}\right] \quad (2)$$

where θ_i and θ_t are the angle of refraction of the mediums of incidence and transmission respectively.

This process continues until the photon exits the medium or has traveled longer than a predefined period of time.

The same rules used previously for the standard MC code to describe photon migration are adopted for the 3D MC code. The tissue is divided into voxels, each of which may have different optical properties. In our simulation, before the photons start to emit, we created a matrix to record the spatial arrangement of tissue constituents. Each voxel in the matrix is assigned an integer to represent the type of tissue in this voxel. As the photon is propagated from one scattering event to the next, a check is made every 1 grid element of 1 mm spacing to see if the scattering or absorption coefficient has changed. Given the initial position and direction of the photon, the length to the first scattering event is calculated. The effect of absorption in each voxel is considered by decreasing the photon weight by $exp(-\mu_a L_j)$ where L_j is the length travelled by the photon (partial path length) through a voxel j. Each photon repeats the free propagation and scattering steps until the present maximal path length is reached or the photon crosses the boundary. If the latter occurs, then the photon position is checked to see if it is detected.

C. Calculation of Spatial Sensitivity profile

In Monte Carlo method, the intensity of the detected light can be determined by taking the sum of the weight coefficients of all photons arriving at the detector, since the weight coefficient W corresponding to the light intensity.

The propagation distance of the photon (average optical path length) travelled by the detected photon i within region j of the tissue types is defined as [2], [11]:

$$L_{i,j} = \frac{\partial A}{\partial \mu_{a,j}} \quad (3)$$

where $A = -ln(\Phi/\Phi_0)$ is the attenuation change in the detected intensity Φ and Φ_0 is the incident radiation.

The sensitivity represents the extent to which the detected signal is affected by a change of absorption due to blood flow or oxygen consumption in a small region of tissue. Equation (3) can be used to calculate the spatial sensitivity profile (SSP) which depends on the probability of a detected photon i travelling within a particular voxel j at position r

from the source optode to the detector optode. The SSP can be derived by taking the sum of the propagations paths of all photons arriving at the detector, weighted by light intensity:

$$SSP(r) \equiv \sum L_{i,j}(r) \quad (4)$$

III. Results and Discussion

We simulated the spatial sensitivity profiles SSP, so-called banana-shaped photon distribution, at various source-detector spacings in order to determine the contribution of the photons scattered from the different regions within the head model as function of separation distance between the source light and the detector location. We run 10^8 photons for all MC simulations to achieve an appropriate SNR for the results presented in this paper. The migrating of all 10^8 photons was performed in a single 3D MC simulation for the two detectors at same time and each simulation took a few hours. The SSP was calculated for each source-detector separation in the head model.

Fig. 2 to Fig. 5 show a cross section of the SSP (banana-shaped photon distribution) across the 3D segmented MR image as well as the contours of the photon visit probability maps for the source-detector separations S-D1 and S-D2 (of 20 and 34 mm respectively), with different values of the reduced scattering coefficient of the CSF $\mu_s' = 0.01$ mm^{-1} and $\mu_s' = 1$ mm^{-1}.

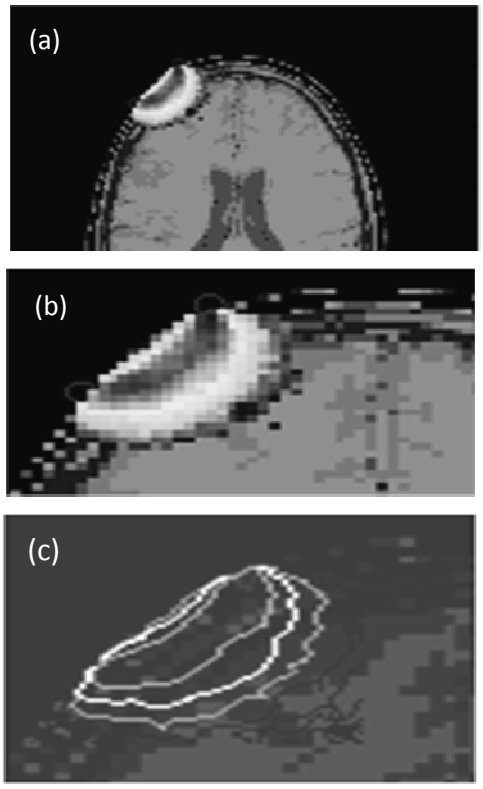

Fig. 2. (a) Banana-shaped photon distribution for the source-detector pair S-D1 separated by 20 mm with $\mu_s' = 1$ mm^{-1}. (b) Zoom on the banana-shaped in (a). (c) The contours of the photon visit probability maps for a source-detector separation S-D1.

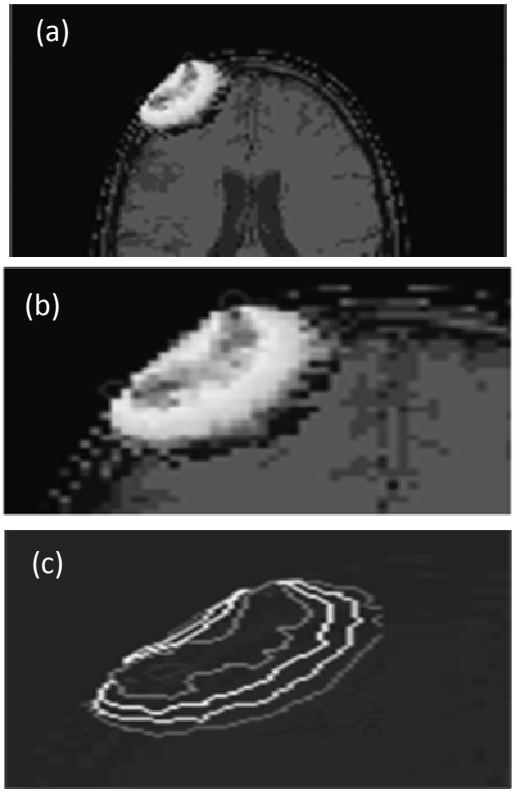

Fig. 3. (a) Banana-shaped photon distribution for the source-detector pair S-D1 separated by 20 mm with $\mu_s' = 0.01$ mm^{-1}. (b) Zoom on the banana-shaped in (a). (c) The contours of the photon visit probability maps for a source-detector separation S-D1.

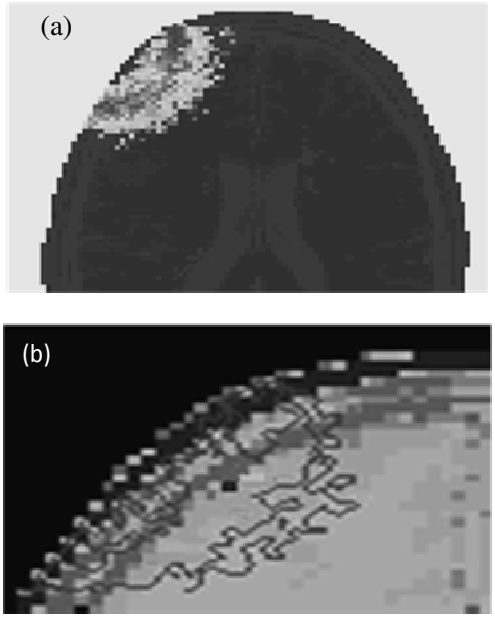

Fig. 4. (a) Banana-shaped photon distribution for the source-detector pair S-D2 separated by 34 mm with $\mu_s' = 1$ mm^{-1}. (b) The contours of the photon visit probability maps for a source-detector separation S-D2.

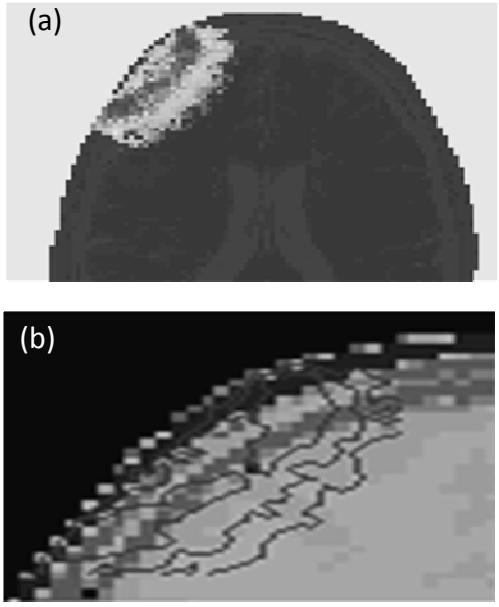

Fig. 5. (a) Banana-shaped photon distribution for the source-detector pair S-D2 separated by 34 mm with μ_s' =0.01 mm^{-1}. (b) The contours of the photon visit probability maps for a source-detector separation S-D2.

The sensitivity to deeper regions seems to vary between different source-detector spacings. For the smaller optode spacing (S-D1 = 20 mm) the minimum depth is obtained and the majority of the detected photons were scattered only in the scalp-skull layer (see Fig. 2 and Fig. 3). However, large distance spacing (S-D2 = 34 mm) will increase light penetration into the brain but intensity of the detected light decreases more strongly, as shown in Fig. 4 and Fig. 5.

In addition, the detected signal depends also on the value of the scattering coefficient of CSF layer. In the case of weak value (μ_s' = 0.01 mm^{-1}), the ratio of photons scattering through brain decreases, whereas most of the light is detected from the scalp-skull layer. Besides, a significant number of photons were guided along the CSF layer, which has the effect of concentrating measurement sensitivity to the more superficial layer (scalp-skull) and may change the depth sensitivity profile. This is consistent with the hypothesis that the sensitivity will change as the scattering length becomes smaller than the typical line-of-sight through the CSF [3], [4], [9]. For a large optode spacing and high value of CSF (μ_s' = 1 mm^{-1}), as shown in Fig. 4, the banana-shaped shows good depth sensitivity to the measurement signal.

The present study has demonstrated that the path length is strongly dependent on the thickness and the optical properties of the superficial tissues and the CSF in the head model. This indicates that the contribution of the extra-cerebral layers to the radiation distribution is large, while the contribution of the brain is small. Thus the estimation of the optical path travelled by photons between the source and the detector is crucial for evaluating the sensitivity of NIRS signals to the brain.

IV. CONCLUSION

Through an analysis of the banana-shaped photon distribution using both MC simulations in 2D head models and in an accurate MRI-based 3D head geometry, we found that the optical properties and thicknesses of the CSF and superficial tissues may influence the diffuse optical imaging (DOI) measurement sensitivity to brain. This means that very low scattering values of CSF should be taken into account when modeling light propagation in the human head. Future studies, of quantification of NIRS measurements during brain activation should focus on the issues of quantification and separation of signals arising from the cerebral tissue from those in the extra-cerebral tissue.

REFERENCES

[1] A. Villringer, J. Planck, C. Hock, L. Schleinkofer, and U. Dirnagl, "Near infrared spectroscopy (NIRS): a new tool to study hemodynamic changes during activation of brain function in human adults," *Neurosci. Lett.*, vol. 154, pp. 101–104, 1993.

[2] E. Okada, M. Firbank, M. Schweiger, S. R. Arridge, M. Cope, and D. T. Delpy, "Theoretical and experimental investigation of near-infrared light propagation in a model of the adult head," *App. Opt.*, vol. 36, pp. 21–31, 1997.

[3] A. H. Barnett, J. P. Culver, A. G. Sorensen, A. Dale , and D. A. Boas, "Robust inference of baseline optical properties of the human head with three-dimensional segmentation from magnetic resonance imaging," *App. Opt.*, vol. 42, pp. 3095–3106, 2003.

[4] A. Custo, W. M. Wells, A. H. Barnett, E. M. C. Hillman, and D. A. Boas, "Effective scattering coefficient of the cerebral spinal fluid in adult head models for diffuse optical imaging," *App. Opt.*, vol. 45, pp. 4747–4755, 2006.

[5] J. Heiskala, T. Neuvonen, P. E. Grant, and I. Nissilä, Significance of tissue anisotropy in optical tomography of the infant brain," *App. Opt.*, vol. 4, pp. 1633–1640, 2007.

[6] Y. Hoshi and M. Tamura, "Detection of dynamic changes in cerebral oxygenation coupled to neuronal function during mental work in man," *Neurosci. Lett*. vol. 150, pp. 5–8, 1993.

[7] B. Montcel, R. Chabrier, and P. Poulet, "Concentration difference maps: a method to retrieve depth-related information on cerebral hemodynamics," *J. Opt. Soc. Am. A*., vol. 14, pp. 12271–12287, 2006.

[8] N. H. Kashou, R. Xu, Cynthia J. Roberts, and L. E. Leguire, "Using FMRI and FNIRS for localization and monitoring of visual cortex activities," *Int. Con. IEEE EMBS Proc.*, vol. 1, pp. 2634–2638, 2007.

[9] C. Mansouri, and J. P. L'Huillier, "Time-resolved photon migration through an adult head model: comparison between Finite Element and Monte Carlo calculations," *SPIE Proc*., *Therapeutic Laser applications and Laser-Tissue Interactions III*, vol. 6632, pp. 66320L1–8, 2007.

[10] L. Wang, and S. L. Jacques, "MCML-Monte Carlo modelling of light transport in multi-layered tissues," *Comput. Methods. Programs. Biomed*., vol. 47, pp. 131–146, 1995.

[11] Y. Hoshi, M. Shimada, Chie Sato and Y. Igushi, "reevaluation of near-infrared light propagation in the adult human head: implications for functional near-infrared spectroscopy," *J. Biomed. Opt*., vol. 10, pp. 064032-3–-064032-10, 2005.